Supporting Online Material for

Marine Polyphosphate: A Key Player in Geologic Phosphorus Sequestration

Julia Diaz, Ellery Ingall,* Claudia Benitez-Nelson, David Paterson, Martin D. de Jonge, Ian McNulty, Jay A. Brandes

*To whom correspondence should be addressed. E-mail: ingall@eas.gatech.edu

Published 2 May 2008, *Science* **320**, 652 (2008)
DOI: 10.1126/science.1151751

This PDF file includes:

Supporting Online Material

Materials and Methods

Field Site and Sampling

Samples were obtained from the upper basin (49° 04.4N, 125° 09.5W) of Effingham Inlet, a Pacific fjord located on the southwestern coast of Vancouver Island, British Columbia, Canada during two cruises conducted in April and July 2007 (Fig. S2). Sample collection included plankton, dissolved material, particles, and underlying sediments.

Plankton were collected using a plankton net (30μm mesh) in surface (<3m) waters. Two large volume (50 and 120 L) seawater samples were collected over several casts of a Niskin bottle rossette for processing by electrodialysis/reverse osmosis. Sinking particles were collected in a sediment trap positioned at a depth of 45m (120m station depth). A multi-corer was used to collect underlying sediments.

X-ray Spectromicroscopy

X-ray spectromicroscopy is a unique methodological tool among techniques currently available in the field of earth science. Specifically, X-ray spectromicroscopy is capable of imaging elemental distributions and determining chemical speciation within minimally-prepared particulate samples. The high spatial resolution achieved with this technique (<1μm) makes the method particularly relevant to the study of micro-scale transformations involved in microbially-mediated processes. X-ray spectroscopy has also been recently applied in several marine carbon and iron cycle studies (e.g., *1-4*).

Sub-micron scale X-ray spectromicroscopy techniques are currently only available at synchrotron radiation facilities, which are uniquely capable of producing sufficiently bright X-

ray beams for micro-scale X-ray spectromicroscopic work. A wide variety of instrument capabilities are possible among synchrotron X-ray spectromicroscopy beamlines worldwide; thus, analytical protocols are highly beamline-specific, and the prospective user has many different instrumentation options. Most synchrotron facilities make instrument time available to users through a competitive application process.

In principle, the X-ray spectromicroscopy technique relies on the quantized interaction of monochromatic X-rays with an element's electrons, typically the inner k-shell electrons. Each element absorbs/fluoresces X-rays at a specific k-edge corresponding to the energy at which the k-shell electrons are bound. Elemental distribution maps are generated by probing a defined sample area with a highly focused, monochromatic X-ray beam of sufficient energy and then detecting element-specific fluorescent X-rays with a multi-element fluorescence detector. Many elements can be mapped and quantified simultaneously.

Chemical speciation is determined by further analyzing particles identified in elemental maps using spectroscopic mode (X-ray Absorption Near Edge Spectroscopy, XANES; or Near Edge X-ray Fluorescence Spectroscopy, NEXFS). In spectroscopic mode, the X-ray beam is focused on a specific region, and the incident energy is varied within a fixed range about the k-edge energy of interest. In the resulting spectra, intensity is expressed as a function of energy; higher energy features depict the local bonding environment around the element of interest and are therefore species-specific. Other species-specific spectroscopic features also exist. For example, with respect to phosphorus, diagnostic shifts in k-edge position occur between organic phases. Myneni 2002 (*5*) and Brandes et al. 2007 (*6*) demonstrated that a wide range of different phosphorus-containing phases (including mineral, organic, and polymeric forms) can be identified by using the spectroscopic "fingerprints" generated with this technique. Although

spectroscopic differences between various phosphorus phases may be subtle, the patterns are consistent and can be easily used to distinguish between different particulate phosphorus phases. Further details on the principles of X-ray spectromicroscopy are available in Myneni 2002 (*5*).

Material for X-ray analysis was obtained from preserved sediment cores (freeze dried and ground) taken from our field site in Effingham Inlet, British Columbia. To prepare samples for analysis, a few milligrams of crude dry sediment were suspended in approximately 100μL of deionized water. Aliquots of this mixture were then mounted onto formvar/carbon-supported copper Transmission Electron Microscopy (TEM) grids that had been adhered to aluminum mounting supports (Fig. S5). Sample mounts were photographed on a standard laboratory light microscope and allowed to dry prior to X-ray analysis.

X-ray surveys of sedimentary phosphorus content were performed with the scanning X-ray microscope (SXM) at beamline 2-ID-B, Advanced Photon Source, Argonne National Laboratory (*7*). This microscope was used to obtain elemental maps at ~60nm spatial resolution, in addition to spectroscopic data from particulate specimens. The beamline operates within the 1-4keV energy range, and can map Na, Mg, Al, Si, P, S, and Cl. Details on the specifications of 2-ID-B are available in McNulty et al. 2003 (*8*).

Specimens were mounted in the SXM using a magnetic stage. Prior to analysis, regions of interest were identified by obtaining coordinates using an in-line visible-light microscope. The visible-light microscope was replaced with an absolutely calibrated photodiode (ACP) for X-ray analysis in order to monitor bulk X-ray transmission through the specimen. A Fresnel zone plate and order-sorting aperture were used to focus a bright X-ray beam into a 60nm spot. Fluorescence from the specimen was measured using a silicon drift diode detector oriented approximately 15 degrees relative to the sample plane. In order to prevent atmospheric

backscatter, specimens were bathed in a continuous helium stream. Fig. S6 depicts the instrument set-up.

Elemental distribution maps spanning several hundred square microns were acquired using 2190eV X-rays and a per-pixel dwell time of 0.5 seconds. Elemental maps revealed sub-micron sized phosphorus-rich domains that were then analyzed spectroscopically. To generate phosphorus NEXFS spectra, high concentration phosphorus regions were interrogated over the 2130-2190eV range at 0.25eV energy intervals using a dwell time of 1.0 second. The dwell times used in our experiments were sufficiently low to avoid significant irradiative damage. Raw X-ray spectroscopy data were normalized relative to the fluorescence signal of the carbon/formvar backing. Spectra were characterized based on the standard library of mineral, organic, and inorganic phosphorus species presented in Brandes et al. 2007 (*6*). Additional standard phosphorus NEXFS data are accessible via the online version of Brandes et al. 2007 (*6)* maintained by the journal *Marine Chemistry*. Figs. S7 and S8 provide standard mineral and polyphosphate spectra relevant to this study.

Important to note is the currently non-quantitative nature of the X-ray spectromicroscopy method. As evident in the current work, the methodological strength of X-ray spectromicroscopy currently lies within its ability to determine speciation and the spatial organization of species within a sample, rather than in any quantitative measurements that the method may be forced to produce. For example, in contrast to more conventional bulk and broad beam spectroscopic studies, spectral modeling of our micro-NEXFS spectra is limited. The position of peaks in NEXFS spectra collected from sub-micron sized particles are highly consistent between identical samples; however, the intensity/amplitude of those peaks varies somewhat between identical samples because the photon flux varies throughout the duration of

the NEXFS scan, for reasons related to the optical behavior of an X-ray beam using zone plate optics: The position of the X-ray focus changes as a function of incident X-ray energy/wavelength. A micron-sized sample located at a fixed position in space will therefore receive a variable cross-sectional area of light (and therefore photon flux) from a micro X-ray beam throughout an energy scan. The variable photon flux issue is not an obstacle in bulk samples for which spectral modeling is a conventional mode of analysis, and the simple optics employed at such instruments are typically of a type that do not alter focus with energy shifts. In focused operation using zone-plate optics, the Z position of the sample has to be actively varied over the course of a spectral scan in order to maintain a constant X-ray spot size on the sample. Moving the sample in Z introduces errors in X and Y as there is unavoidable wobble on the order of up to several microns. The two ways in which this problem has been tackled are as follows: first, taking many images at different incident energies (impractical for fluorescence studies) with subsequent software alignment, and second, laser interferometer correction for sample position (expensive and not available at 2-ID-B). Thus, due to time and resource constraints, the microscope at 2-ID-B is operated with fixed Z position during spectral scans. Because of the methodological effect of variable photon flux, any modeling results of micro-NEXFS spectra collected under the above conditions would produce significant experimental artifacts.

Electrodialysis/Reverse Osmosis

The combined process of electrodialysis and reverse osmosis (ED/RO) isolates molecules dissolved in seawater by first desalinating and then concentrating high volume (>50 L) samples. Samples for ED/RO were taken at depths of 61 and 78 m from our sampling site in Effingham Inlet during both cruises in April and July 2007.

As the first step in ED/RO, electrodialysis is used to remove ions from the seawater sample (Fig. S9). In electrodialysis, the seawater sample (to be deionized) is contacted with a concentrate flow (to receive ions) across many pairs of cation and anion exchange membranes. A DC electrical current is directed through the membrane stack. Only ionized dissolved components are targeted by ED. The ion exchange membranes are non-porous above the size of the interstitial spaces between the polymer chains in the cross-linked hydrated ion exchange resin. The process results in a concentrate solution, which is discarded, and a deionized solution (diluate). The diluate solution is subsequently concentrated via RO in order to isolate dissolved molecules for analysis.

In RO, a feed solution consisting of water and aqueous solutes is placed under pressure and pumped from a sample reservoir across a semi-permeable RO membrane, where the feed solution is separated into a permeate solution (relatively lower concentrations of solutes) and a retentate solution (relatively higher concentrations of solutes). When RO is being used to concentrate solutes from the feed solution, the retentate solution is recycled back to the sample reservoir and the permeate solution is discarded. As more feed solution is added either continuously or discontinuously to the sample reservoir, the concentrations of all solutes, including dissolved organic molecules that are rejected by the membrane, gradually increase in the sample reservoir.

Conventional ultrafiltration methods that do not desalinate seawater samples can only isolate the high molecular weight fraction (>1kDa) of dissolved matter, which comprises only ~30% of total dissolved matter. By comparison, ED/RO is capable of yielding salt-free samples consisting of both high and low molecular weight dissolved matter, resulting in up to 90% recoveries. The high recoveries capable through ED/RO enable the characterization of the

chemically distinct low molecular weight species and are therefore key to the comprehensive examination of marine dissolved matter. We recovered ~70% of dissolved matter from our Effingham Inlet samples. See Vetter et al. 2007 (*9*) for further technical details on ED/RO.

Polyphosphate Content—^{31}P-NMR

Plankton samples, sediment trap material, and dissolved matter isolated from ED/RO were freeze-dried and ground. These samples were then analyzed using solid-state ^{31}P-Nuclear Magnetic Resonance (NMR). Solid-state ^{31}P-NMR analyses were carried out at the NMR center in the School of Chemistry and Biochemistry at the Georgia Institute of Technology. The NMR spectra were acquired on a Bruker DSX 400 spectrometer using Cross Polarization-Magic Angle Spinning techniques at a ^{31}P frequency of 161 MHz. Approximately 90 mg of powdered sample was packed into a 4 mm diameter cylindrical zirconia rotor fitted with a Kel-F cap and spun at 10 000±10 Hz in a Bruker magic-angle spinning probe. For all samples, a cross-polarization sequence, optimized to obtain semi-quantitative data, was used with a 1.0 ms contact time and a pulse delay of 4 s. A total of 8192 to 32768 transients were collected for each sample. The data processing and calculation of integrated peak areas were carried out off-line using the Spinworks software package. The errors associated with determination of the abundance of different chemical forms through integration of solid-state NMR peak areas are on the order of ±10% of the reported value (*10-12*). For example, a polyphosphate measurement of 7% would have an associated error of ±0.7%.

Epifluorescence Microscopy

Seawater samples from above and below the photic zone were fixed with a final concentration of 4% formaldehyde. Cells were vacuum-filtered (pressure <10cm Hg) onto

25mm polycarbonate membranes having a nominal pore size of 0.2μm. Filtered samples were stained in the dark for five minutes with ~1mL of 40μgmL^{-1} DAPI (4',6'-Diamidino-2-phenylindole) and subsequently examined and photographed under UV illumination with an Olympus epifluorescence microscope. The fluorescence of nucleus-bound DAPI (emission at 456nm) was sufficiently distinct from the fluorescence signal of polyphosphate-bound DAPI (emission at 525nm) to distinguish between these two DAPI-sensitive inclusions. Numerous independent studies report the use of DAPI as a stain for polyphosphate in eukaryotic algae, e.g., Eixler et al. 2005 (*13*) and Ruiz et al. 2001 (*14*).

Biogenic Silica

Plankton, sediment trap, and underlying sediment samples were treated by the method of Mortloch and Froelich (*15*) in order to dissolve any opal present (error associated with this measurement is <3%). Dissolved Si content was then determined by the method of Hansen and Koroleff (*16*), which has a typical analytical error of ±7%.

Elemental content

Freeze-dried and ground plankton samples were analyzed for C and N content using an elemental combustion system (Costech instruments, model no. ECS4010). The error for this method is typically ±1% (*17*). In order to determine total and inorganic phosphorus content, plankton, dissolved matter, sediment trap, and underlying sediment samples were acidified, combusted, and analyzed according to the Aspila method (*18*). Duplicate samples agreed to within <5%, and the measured value of NIST Standard Reference Material 1573a (tomato leaves) was within ±5% of the certified value.

Soluble Reactive Phosphate

In surface seawater samples, soluble reactive phosphorus was determined spectrophotometrically by using the molybdate method of Koroleff (*19*). Typically errors for this method are <3%.

Sediment Traps

Sinking particles were collected in a sediment trap positioned at a depth of 45m in our ~120m depth field site. The sediment trap (1.5m diameter net) was deployed for 44 hours, from which 1.21g of dried material was collected. We note that our single sediment trap measurement cannot account for long-term variations in particle flux. In addition, as is typical for any oceanographic research, replicate trap deployments were unrealistic given our equipment and sampling time for this study. Thus, any calculations based on our trap measurement are meant to provide broad insights into the dynamics of the natural system, rather than rigorous quantitative assessments.

Supporting Text

A provisional rate for the process of polyphosphate nucleated apatite precipitation in marine sediments may be calculated. Polyphosphate represents 8% of the total phosphorus in 0-3 year-old surface sediments from Effingham Inlet (*20*). The polyphosphate concentration in deeper, 18-20 year-old sediments is below the ^{31}P-NMR detection limit (*20*, *21*) and for the purposes of the current calculation is approximated as zero. Using these two end points, the rate of polyphosphate nucleated apatite growth in sediments is conservatively estimated to be ~0.5% of sedimentary polyphosphate per year.

The ability of X-ray spectromicroscopy to identify polyphosphate in deep Effingham Inlet sediments up to 60 years old highlights the considerable sensitivity and analytical strength of X-ray spectromicroscopy in its ability to identify the presence of low-concentration phases. The X-ray detectable pool of polyphosphate that is present in deeper sediments may be unreactive as a consequence of protective mechanisms involving cation complexation and silica mineral coatings. Regardless of the reactivity differences between mineral-transformed and recalcitrant polyphosphate, however, sedimentary polyphosphate represents a phosphorus sink.

Until now, the accumulation of substantial authigenic apatite in marine sediments has been a fundamental mystery. For example, apatite precipitation is a kinetically-controlled process in most marine sediments, as calcium phosphate minerals are highly insoluble under typical sedimentary conditions and pore waters are therefore commonly supersaturated with respect to apatite (*22*). Yet most marine sediments contain significantly more authigenic apatite than predicted by kinetic porewater precipitation models (*22*).

The polyphosphate template mechanism for apatite formation proposed in this study would produce a dispersed distribution of authigenic apatite in marine sediments based on the observation that polyphosphates appear to be similarly dispersed within the sediments of our field site. This apatite distribution matches the puzzlingly disperse distribution of apatite minerals typically observed in sediments from non-upwelling zones and is thereby the first mechanism to potentially explain the formation of fine-grained apatites in such environments. The potential for polyphosphate as a template for apatite mineral growth in natural systems also gains support from bioengineering research. For example, bone cements enriched with calcium polyphosphate have recently been shown to enhance apatitic bone growth and repair (*23*).

Supporting Figures

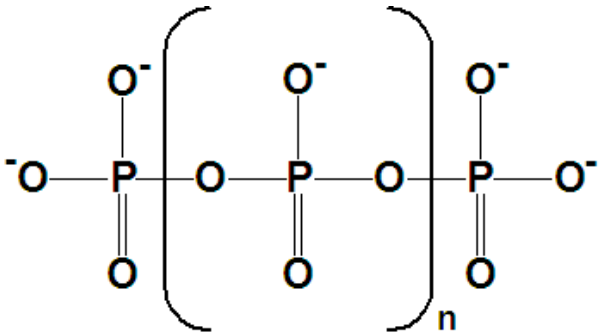

Fig. S1. Polyphosphate molecular structure. Polyphosphate is an unbranched polymer of orthophosphate units (n = 1 to >100) linked by high-energy phosphoanhydride bonds. Owing in part to the nucleophilicity of orthophosphate units, polyphosphate granules are ionically complexed with charge-balancing cations in organisms, especially calcium, a major ion in seawater.

Fig. S2. Effingham Inlet. The study site is circled in red.

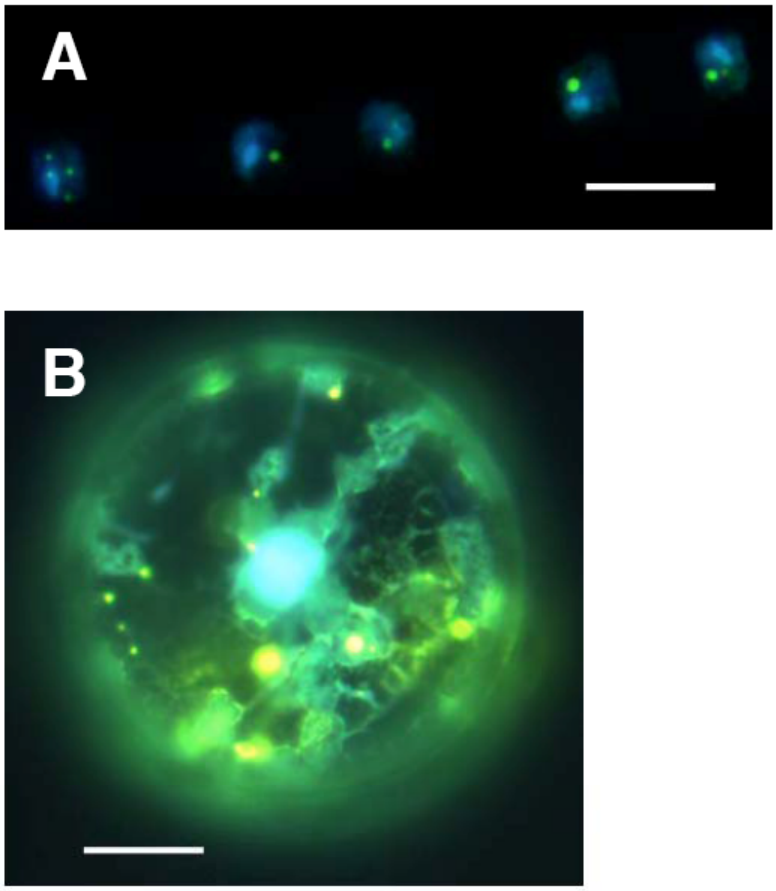

Fig. S3. Polyphosphate in diatoms collected from natural marine waters. Cells collected from the coastal waters of Effingham Inlet, British Columbia, were fixed and stained with the standard fluorochrome 4',6-diamidino-2-phenylindole (DAPI) (*16*). In our samples, DAPI not only revealed cell nuclei (blue) but also many large intracellular polyphosphate inclusions (yellow to green), as seen in (A) *Skeletonema* spp. and (B) a solitary centric diatom. This image shows that plankton collected from natural marine waters synthesize polyphosphate at non-enriched, sub-micromolar dissolved phosphate concentrations that are typical of many regions in the global ocean. Scale bars are 10μm.

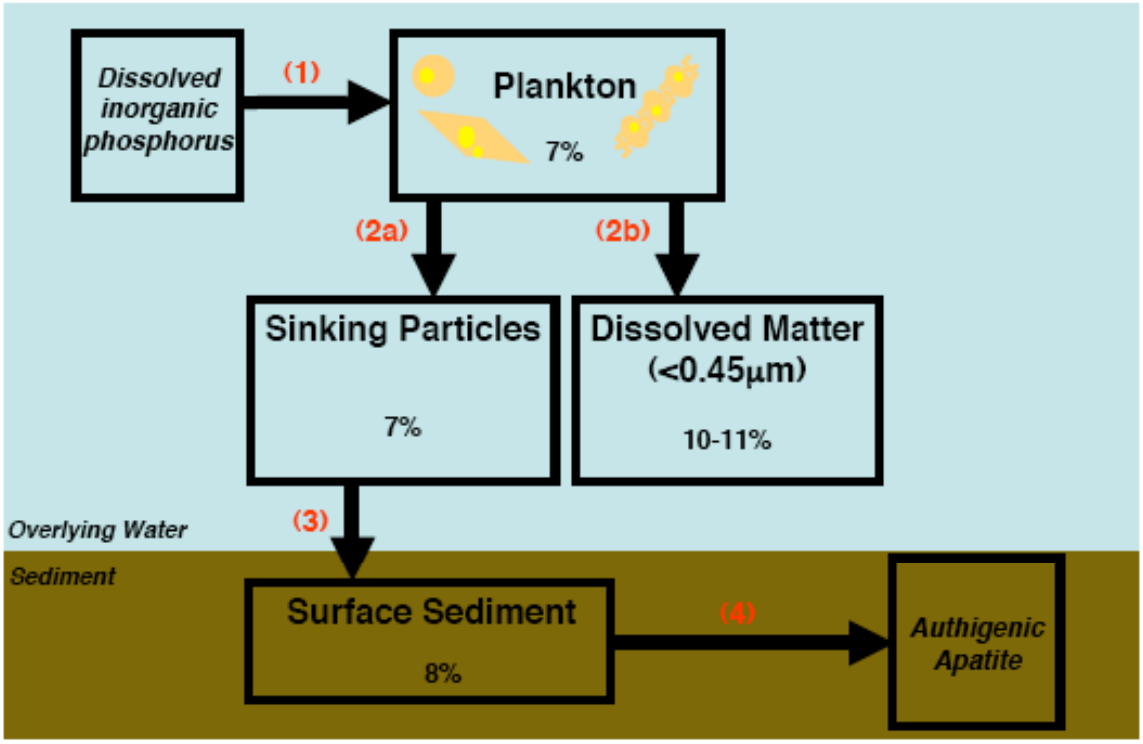

Fig. S4. "Biological pump" mechanism for geologic sequestration of phosphorus. **(1)** Plankton in surface waters assimilate dissolved inorganic phosphorus into intracellular calcium-associated polyphosphate granules. In the bulk plankton community, polyphosphate accounts for 7% of total phosphorus. **(2a)** Intact polyphosphate-rich cells or extracellular polyphosphate particles from the water column sink (polyphosphate represents 7% of the total phosphorus in sinking particles). **(2b)** Alternatively, biogenic polyphosphate derived from plankton growth in the euphotic zone can enter the dissolved phase, in which polyphosphate accounts for 11% of total phosphorus. **(3)** Polyphosphate derived from the water column sinks to surface sediments, where polyphosphate is 8% of total phosphorus. **(4)** In surface sediments, calcium-associated polyphosphate can reduce the kinetic nucleation barrier to the precipitation of calcium phosphate minerals, and diagenetic transformation into fine-grained, geologically stable authigenic apatite particles can thereby occur. Thus, steps 1, 2a, 3, and 4 together constitute a "biological pump" mechanism by which dissolved, water column-derived phosphorus is delivered to underlying sediments and sequestered over geologic timescales as stable mineral phases via an inorganic polyphosphate intermediate.

Fig. S5. SXM Sample Mount. Carbon/formvar-backed copper TEM grids (3mm diameter; Ted Pella™) were attached to the upper and lower holes of aluminum mounting sticks. Milligrams of sediment were deposited onto the TEM grids.

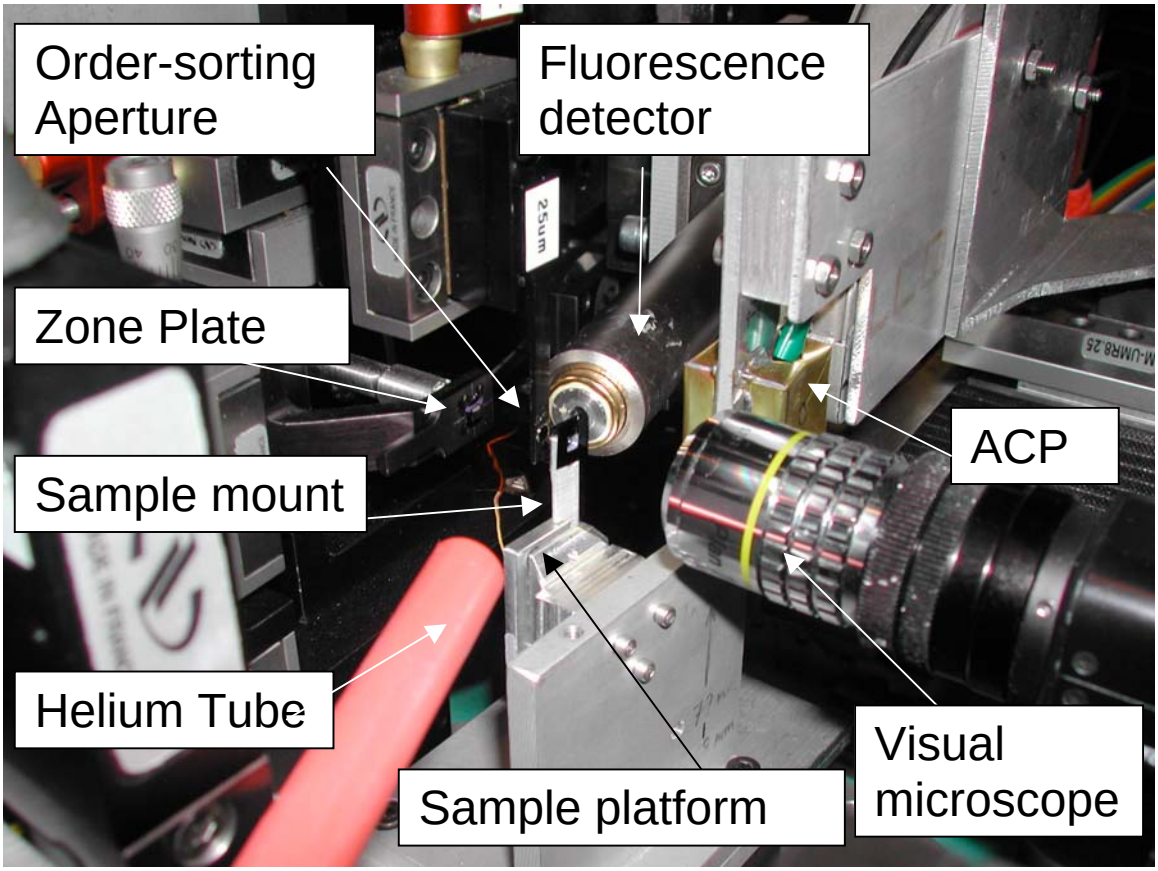

Fig. S6. Instrument set-up at beamline 2-ID-B. Analyses are performed with multiple X-ray detectors and optical components positioned at millimeter to centimeter distances away from the sample. Instruments are moved using high spatial resolution motors. See text for a description of instrument components. Photo courtesy of Juergen Thieme.

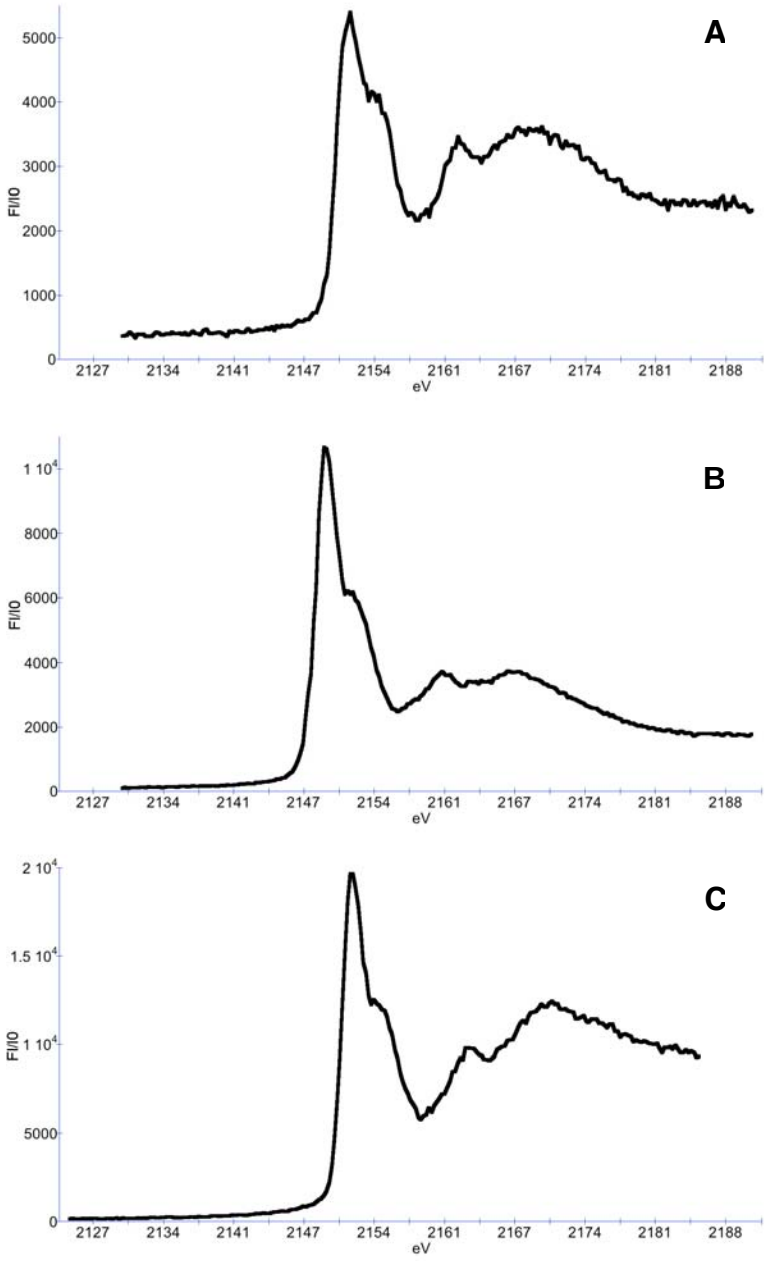

Fig. S7. X-ray fluorescence spectra of standard calcium phosphate mineral phases. Normalized phosphorus X-ray fluorescence spectra of **(A)** carbonate fluorapatite, **(B)** hydroxyapatite, and **(C)** phosphorite are all characterized by a primary peak "shoulder" and two high-energy peaks located at 11eV and 18eV above the primary peak position. Based on our analyses, other calcium phosphate minerals yield subtly different yet distinct phosphorus X-ray fluorescence spectra.

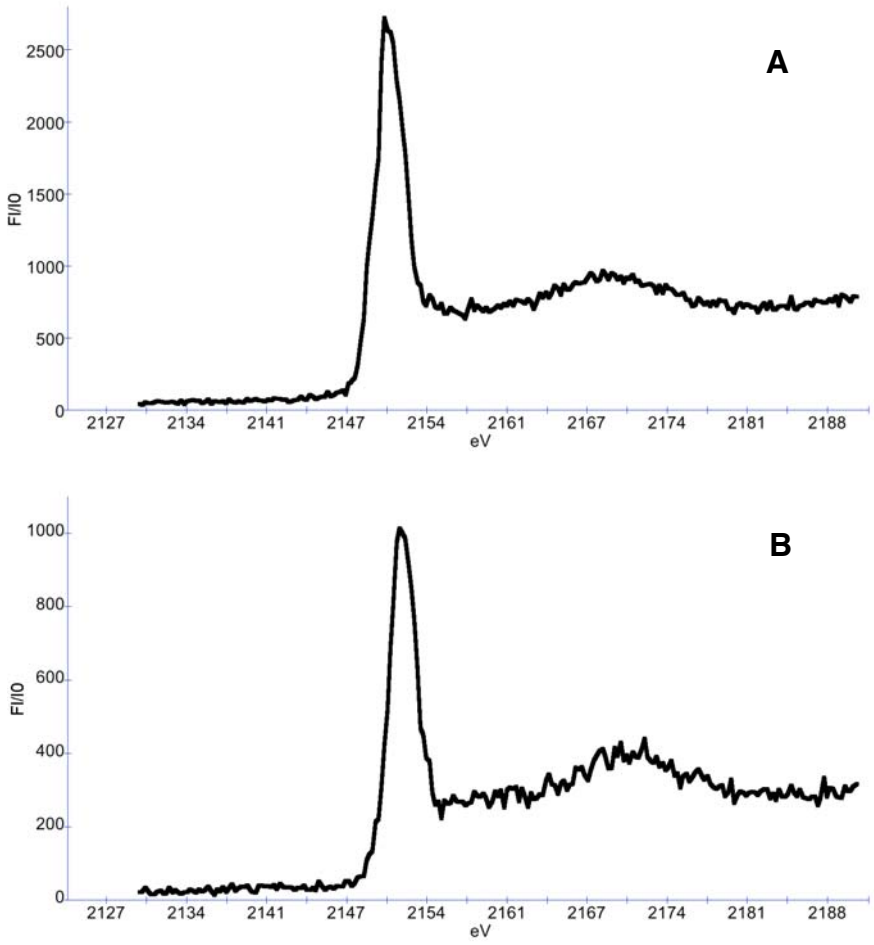

Fig. S8. X-ray fluorescence spectra of standard biogenic polyphosphate. These phosphorus X-ray fluorescence spectra were collected from intracellular polyphosphate granules of the freshwater algae: **(A)** Chlamydomonas sp. and **(B)** Chlorella sp. As shown in these spectra, biogenic polyphosphate yields phosphorus fluorescence spectra characterized by a featureless primary peak and a single high-energy peak located 18eV above the primary peak position.

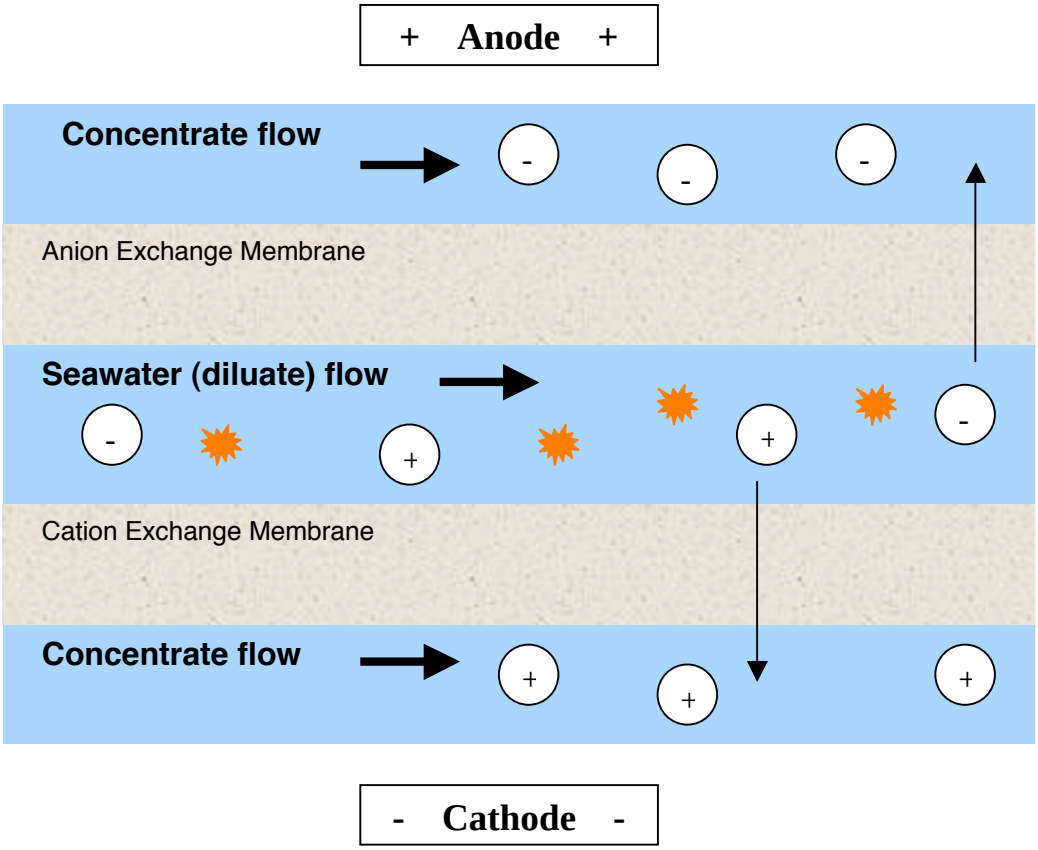

Fig. S9. Electrodialysis. Seawater contacts a concentrate flow across many pairs of anion/cation exchange membranes through which a DC current is directed. In this process, ions move from the seawater flow (diluate) into the concentrate flow, while dissolved molecules (orange globules) are retained in the diluate flow. Dissolved molecules in the salt-free diluate flow are subsequently concentrated using reverse osmosis.

References and Notes

1. J. A. Brandes, C. Lee, S. Wakeham, M. Peterson, C. Jacobsen, S. Wirick, G. Cody, *Mar. Chem.* **92**, 107 (2004).
2. P. J. Lam, J. K. B. Bishop, C. C. Henning, M. A. Marcus, G. A. Waychunas, I. Y. Fung, *Global Biogeochemical Cycles* **20**, GB1006 (2006).
3. B. S. Twining, S. B. Baines, N. S. Fisher, M. R. Landry. *Deep-Sea Research Part I-Oceanographic Research Papers* **51**, 1827 (2004).
4. B. S. Twining et al. *Analytical Chemistry* 75, 3806 (2003).
5. S. C. B. Myneni, *Reviews in Mineralogy & Geochemistry*. pp. 485-579 (2002).
6. J. A. Brandes, E. Ingall, D. Paterson, *Mar. Chem.* **103**, 250 (2007).
7. Use of the Advanced Photon Source is supported by the U.S. Department of Energy, Office of Basic Energy Sciences (DE-AC02-06CH11357).
8. I. McNulty *et al.*, *Journal De Physique IV* **104**, 11 (2003).
9. T. A. Vetter, E. M. Perdue, E. Ingall, J.–F. Koprivnjak, P. H. Pfromm, *Separation and Purification Technology* **56**, 383 (2007).
10. P. Sannigrahi, E. Ingall, *Geochem. Transac*. **6**, 52 (2005).
11. J. I. Hedges, J. A. Baldock, Y. Gelinas, C. Lee, M. L. Peterson, S. G. Wakeham, *Mar. Chem.* **78**, 47 (2002).
12. P. Sannigrahi, E. D. Ingall, R. Benner, *Deep Sea Research* **52**, 1429 (2005).
13. S. Eixler, U. Selig, U. Karsten, *Hydrobiologia* **533**, 135 (2005).
14. F. A. Ruiz, N. Marchesini, M. Seufferheld, Govindjee, R. Docampo, *Journal of Biological Chemistry* **276**, 46196 (2001).
15. R. Mortloch, P. N. Froelich, *Deep Sea Res.* **36**, 1415 (1989).

16. H. P. Hansen, F. Koroleff in *Methods of Seawater Analysis*, K. Grasshoff, K. Kremling, M. Ehrhardt, Eds. (Wiley-VCH, Weinheim, 1999) pp.159.

17. J. I. Hedges, J. H. Stern, *Limnology and Oceanography* **29**: 657 (1984).

18. K. I. Aspila, H. Agemian, A. S. Y. Chau, *Analyst* **101**, 187 (1976).

19. F. Koroleff in *Methods of Seawater Analysis*, K. Grasshoff, K. Kremling, M. Ehrhardt, Eds. (Verlag Chemie, Weinheim, 1983) pp. 125.

20. P. Sannigrahi, E. Ingall, *Geochem. Transac.* **6**, 52 (2005).

21. E. Ingall, L. Kolowith, T. Lyons, M. Hurtgen. *American Journal of Science*. **305**, 240 (2005).

22. P. Van Cappellen, R. A. Berner, *Geochim. Cosmochim. Acta* **55**, 1219 (1991).

23. K. S. Oh *et al.*, *Bioceramics 17 Key Engineering Materials* **284-286**: 93 (2005).